Received: 23 October 2024 | Revised: 6 August 2025 | Accepted: 24 July 2026 | Published online: 17 August 2026

RESEARCH ARTICLE

Journal of Optics and Photonics Research
2026, Vol. 00(00) 1–8
DOI: 10.47852/bonviewJOPR62024617

Enhancing Carrier Suppression in Radio-over-Fiber Links Using Sagnac Loop Techniques

Archa Chandrasenan[1,*], S. J. Anshula Vijayam[1] and Joseph Zacharias[1]

[1] *College of Engineering Trivandrum, APJ Abdul Kalam Technological University, India*

Abstract: We present an optimized technique to improve the optical carrier-to-sideband ratio (OCSR) in a radio-over-fiber (RoF) link using a Sagnac loop configuration. Improving OCSR is important for better power efficiency and efficient bandwidth usage in modern communication systems. The proposed system consists of a Sagnac loop integrated with a $LiNbO_3$ modulator and a polarization splitter. To optimize OCSR, key performance parameters such as extinction ratio (ER), spurious-free dynamic range (SFDR), bit error rate (BER), error vector magnitude (EVM), and signal-to-noise ratio (SNR) are analyzed. Results show that increasing ER plays a major role in enhancing optical carrier suppression. The Sagnac-based RoF system improves SFDR by more than 19 dB over a wide range of radio frequency (RF) frequencies. Although SNR slightly reduces due to power fading compensation, overall system performance improves significantly. Compared to conventional Mach–Zehnder modulators, the proposed design achieves better performance, with an EVM of 12.31%, BER of 0.4765 at high RF power, and a peak SFDR of 113.34 dB·$Hz^{2/3}$ at 20 GHz.

Keywords: carrier suppression ratio, polarization splitter, extinction ratio, spurious-free dynamic range, error vector magnitude

1. Introduction

Radio-over-fiber (RoF) technology enables the transmission of radio frequency (RF) signals through analog optical links. In an RoF system, RF signals are modulated onto an optical carrier (OC) at a central station and then transported to remote locations or base stations (BS) via optical fibers. The BS then broadcasts the RF signal over small regions using microwave antennas [1]. RoF systems are widely preferred in communications because of their lightweight design, low signal loss, high capacity, and robust resistance to electromagnetic interference. Despite the fact that the OC does not hold any actual information [2], it absorbs most of the optical power in a quadrature-biased modulation link. RoF combines the benefits of both fiber-optic and wireless communications. Nonetheless, the process of converting electrical signals to optical ones introduces nonlinear distortion [3], specifically third-order intermodulation distortion (IMD3), into the RF signal. Periodic power fading due to chromatic dispersion also deteriorates the signal-to-noise ratio (SNR) [4]. Nonlinear distortion and power fading significantly degrade the spurious-free dynamic range (SFDR) and limit the applications of RoF systems [5].

The IMD3 has been constrained by introducing an appropriate phase shift into the OC band [6]. Digital post-processing or digital predistortion can suppress IMD3 in the electrical domain [7]. In the optical field, IMD3 suppression can be accomplished by different methods, such as creating a parallel inverse nonlinear distortion link [8], subjecting the OC to the proper phase shift [9], adjusting the power distribution of the system [10], or maintaining the polarization state of the system [11]. Moreover, an integrated dual-drive dual-parallel Mach–Zehnder modulator (MZM) [12] can be used to suppress IMD3 [13]. Also, a fiber Bragg grating along with a dispersive fiber is used to nullify the effect of IMD3.

Various studies are being conducted to prevent wavelength-dependent distortion and periodic power fading [14]. Wavelength-dependent distortion will eventually alter the phase of the RF signal by forming its Hilbert transform [15]. Periodic power fading can be prevented by adjusting the polarization controller (PC) prior to the modulator. The periodic power fading can be compensated using a Sagnac loop by controlling the phase difference between the two sidebands. This eliminates periodic power fading and lowers the power of the orthogonally polarized carrier, which is generated by fading. Further, the bias of the modulator is also adjusted to counteract periodic power fading.

Recently, more research has been done to concurrently reduce both periodic power fading and IMD3. To achieve link linearization, a sufficient phase shift is introduced into the OC band. Hence, IMD3 can be suppressed and power fading reduced by adding a sufficient phase shift between the odd and even sidebands. However, none can completely prevent the effect, though they reduce the effects of periodic power fading. By biasing the modulator at the minimum point and adding an extra OC, IMD3 is mitigated. Periodic power fading can be prevented by modifying the phase difference between the OC and sidebands. It is noted that certain IMD3 portions cannot be suppressed. Transmission performance can be maximized by using an optimal

***Corresponding author:** Archa Chandrasenan, College of Engineering Trivandrum, APJ Abdul Kalam Technological University, India. Email: archachandrasenan@cet.ac.in

optical carrier-to-sideband ratio (OCSR). The OCSR is optimized by adjusting the angle between the signal and the polarizer (Pol). To maximize the OCSR, the bias voltages of the dual-polarization MZM are adjusted, and to further enhance the OCSR, the two polarized light beams are rotated by a PC. By utilizing cascaded polarization modulators, a tunable OCSR is achieved. In this paper, a Sagnac loop with a lithium niobate ($LiNbO_3$) MZM and a polarization splitter is designed to achieve better carrier suppression compared to traditional MZM modulators. The Sagnac loop utilizes two light waves traveling in clockwise (CW) and counterclockwise (CCW) directions. In the CCW direction, the light is modulated with the carrier signal, while in the CW direction, the light is suppressed. This configuration reduces power fading and improves signal efficiency. The optimized optical carrier-to-sideband ratio (OCSR) significantly enhances the performance of the RoF link, assessed through various parameters such as the modulator's extinction ratio (ER), SFDR, bit error rate (BER), error vector magnitude (EVM), and SNR. SFDR is a critical parameter that depends on the noise floor, gain, and noise figure and is commonly used in radio receivers to determine the range of input power for noise-free signal detection and amplification without nonlinear distortion. The ER, defined as the ratio between two optical power levels of a digital signal produced by an optical source, indicates better carrier suppression with higher values. As a result, the proposed link demonstrates lower EVM and BER at higher input RF power levels, confirming that the RoF system design achieves a better OCSR compared to previous methods. This novel system approach provides tunable carrier suppression ratio (CSR), contrasting with methods such as simply adjusting the modulator's direct current (DC) bias or achieving tunable CSR by adjusting the PC in Wu et al. [16]. The standout feature of the proposed system is its lower EVM and BER at higher input RF power, confirming superior OCSR performance over previous techniques. The proposed link demonstrates an EVM of 12.31% and a BER of 0.4765 at a 20 GHz input signal frequency, significantly improving over prior methods and showing strong potential for enhanced tunable CSR performance [17].

We propose an optimized RoF link that enhances the OCSR using a Sagnac loop. Optimizing OCSR is essential for improving power efficiency and bandwidth utilization in communication systems. The system is built with a $LiNbO_3$ modulator and a polarization splitter to construct the Sagnac loop. Key performance metrics such as ER, SFDR, BER, and SNR are optimized to achieve a significant enhancement in OCSR, leading to more efficient and reliable RoF communication.

The paper is organized as follows: Section 2 describes the design and analysis of the proposed system. Section 3 presents the obtained results and evaluations. Finally, Section 4 concludes the paper.

2. System Design

The schematic diagram of the proposed RoF link is illustrated in Figure 1. Light generated by a laser diode is directed into a Sagnac loop through a PC and an optical circulator. The circulator has three ports: port 1 is connected to the output of the PC, port 2 is linked to the Sagnac loop—comprising a polarization beam splitter (PBS) and a lithium niobate ($LiNbO_3$) MZM for carrier suppression, and port 3 is connected to the input of the phase shifter [18]. The signal undergoes phase shifting to achieve orthogonality, thereby reducing dispersion effects. This attenuated signal is further adjusted by passing it through a PC, and its power is subsequently amplified using an erbium-doped fiber amplifier (EDFA). Finally, a photodiode converts the optical signal into an electrical signal [19].

2.1. Optimization of optical carrier-to-sideband ratio

The lithium niobate ($LiNbO_3$) MZM is biased to ensure that the OC components are canceled at its output. The optical signal generated at the output of the MZM is represented by Equation (1):

$$E_{out}(t) = E_0 \cos[\pi V(t)/2V_{\Pi}] \cos(\omega_c t) \tag{1}$$

where E_0 and ω_c are the amplitude part and angular frequency part of the input OC, respectively. V_π is the half-wave voltage of the modulator. It is crucial in determining the efficiency of phase modulators, such as those used in electro-optic modulation systems [20]. $V(t)$ is the applied driving voltage; it consists of an electrical sinusoidal signal and a DC-biased voltage, as given by Equation (2):

$$V(t) = V_{bias} + V_m \cos(\omega_{RF} t) \tag{2}$$

where V_{bias} is the biased voltage and V_m and ω_{RF} are the modulation voltage and the angular frequency of the electrical driving signal, respectively. The output of the modulator converted from exponentials to sinusoidal results in Equation (3):

$$\begin{aligned} E_{out}(t) &= E_0 \cos(\pi/2[V_{bias}/V_\pi \\ &\quad + V_m/V_\pi \cos(\omega_{RF} t)]) \cos(\omega_c t) \\ &= E_0 (Cosx.cos[mcos(\omega_{RF} t)] \\ &\quad - sinx.sin(mcos(\omega_{RF} t))) \cos(\omega_c t) \end{aligned} \tag{3}$$

Figure 1
Schematic diagram of the proposed optimized RoF link

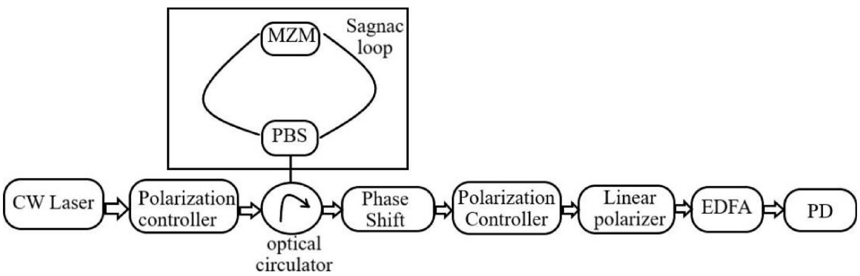

Note: PBS: polarization beam splitter, MZM: Mach–Zehnder modulator, EDFA: erbium-doped fiber amplifier, PD: photodetector.

where $x = (V_{bias}/2V_{\pi})\pi$ is a constant phase shift that is induced by the DC-biased voltage and m $= (V_m/2V_{\pi})\pi$ is the phase modulation index.

Equation (3) can be rewritten in terms of the Bessel function. The output of the modulator in terms of the Bessel function is given by Equation (4):

$$\begin{aligned} E_{out}(t) = E_0 \cos x(J_0(m)\cos(\omega_c t) \\ + \sum_{n=1}^{\infty}[J_2 n(m)\cos(\omega_c t + 2n\omega_{RF}t - n\pi) \\ + J_2 n(m)\cos(\omega_c t - 2n\omega_R st + n\pi)]) \end{aligned} \tag{4}$$

where J_n is the Bessel function of the first order n. The initial term in this equation represents the carrier component, while the subsequent terms correspond to the odd-order and even-order sidebands, respectively. If the bias voltage equals the driving voltage, $Vb_{ias} = V\pi$, then $\cos x = 0$ and $\sin x = 1$, as $x = (Vb_{ias}/2\ V\pi)\ \pi$. The modulator's output with suppressed carrier is given by Equation (5).

$$\begin{aligned} E_{out}(t) = E_0(\sum_{n=1}^{\infty}[J_{2n-1}(m)\cos(\omega_c t + 2n\omega_{RF}t - n\pi) \\ + J_{2n-1}(m)\cos(\omega_c t - 2n\omega_{RF}t + n\pi)) \end{aligned} \tag{5}$$

It is evident that the performance of the RoF system improves after the carrier signal is suppressed. SFDR is a crucial performance metric in many systems. SFDR is defined as the range between the minimum detectable signal level and the point where the third-order intermodulation product (noise) exceeds the minimum detection level [21]. Essentially, SFDR indicates the maximum SNR achievable within a system, making it a vital measure of performance. It is given by Equation (6):

$$SFDR = \frac{2}{3}(IMD3 - MDS) \tag{6}$$

where MDS is the minimum detectable signal in dBm. Minimum detectable signal (MDS) is the lowest signal power level that a receiver can detect and process above the background noise to yield the necessary output. For accurate detection, the signal power level must surpass the noise floor or background noise. MDS is expressed as Equation (7).

$$\begin{aligned} MDS = 10 \times log_{10}(\frac{kT}{1mW}) \\ + NoiseFigure + 10 \times log_{10}(Bandwith) \end{aligned} \tag{7}$$

where T is the temperature in K, k is Boltzmann's constant (228 dBW/(K·Hz)), noise figure is expressed in dB, and bandwidth is expressed in Hz/MHz/GHz.

OCSR is calculated based on the expression given by Equation (8):

$$CSR = \frac{P_{oc}}{P_{+1}} \tag{8}$$

where P_{oc} is the OC power and P_{+1} is the 1^{st}-order sideband power.

The Sagnac loop works by splitting light into two counter-propagating beams, and the phase shift between them, caused by rotation, is used to measure angular velocity. Polarization control is crucial to ensure accurate operation, as fiber-optic systems are sensitive to polarization-dependent losses and phase shifts. A PC before the loop sets the input polarization, ensuring both beams have the same initial polarization, while a second PC after the loop aligns the output polarization for optimal recombination. This ensures that polarization mismatches do not distort the interference pattern, leading to precise rotation measurements.

3. Research Methodology

The experimental setup begins with a laser source operating at a wavelength of 1550 nm, analyzed using an optical spectrum analyzer to verify the spectral characteristics of the generated optical signals. These signals are routed through a PC and an optical circulator before reaching the PBS. The $LiNbO_3$ MZM employed in the system exhibits an insertion loss of 6.5 dB and a switching bias voltage of 4 V, with a biasing range from –2 V to 2 V. A key design parameter—ER—is optimized at 35 dB to achieve efficient optical carrier suppression (OCS).

To test the system's modulation performance, a two-tone microwave signal comprising 5 GHz and 10 GHz components is fed to the modulator's RF input. These tones are phase-shifted and assigned orthogonal polarization states. By precisely

Figure 2
(a) Optical spectra with suppressed carrier obtained at the output of the Sagnac loop and (b) frequency response characteristics of the proposed system based on the Sagnac loop and the conventional system based on MZM

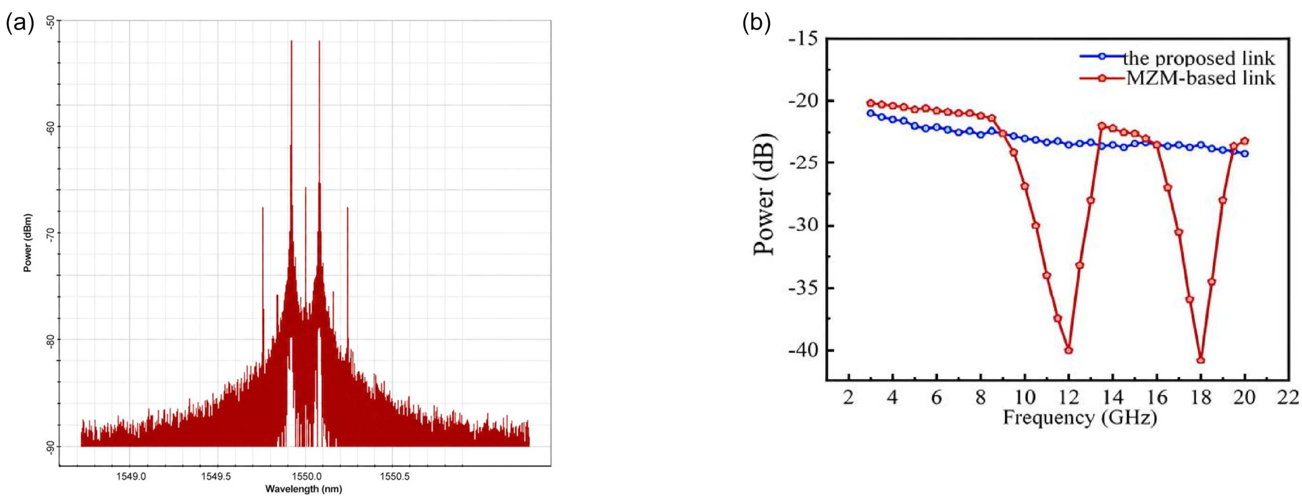

Figure 3
Optical spectrum obtained at the output of the Sagnac loop, showing the extent of carrier suppression by varying the value of ER at (a) 15 dB, (b) 20 dB, (c) 25 dB, (d) 30 dB, and (e) 35 dB; (f) variation of CSR (dB) with respect to different values of ER (dB)

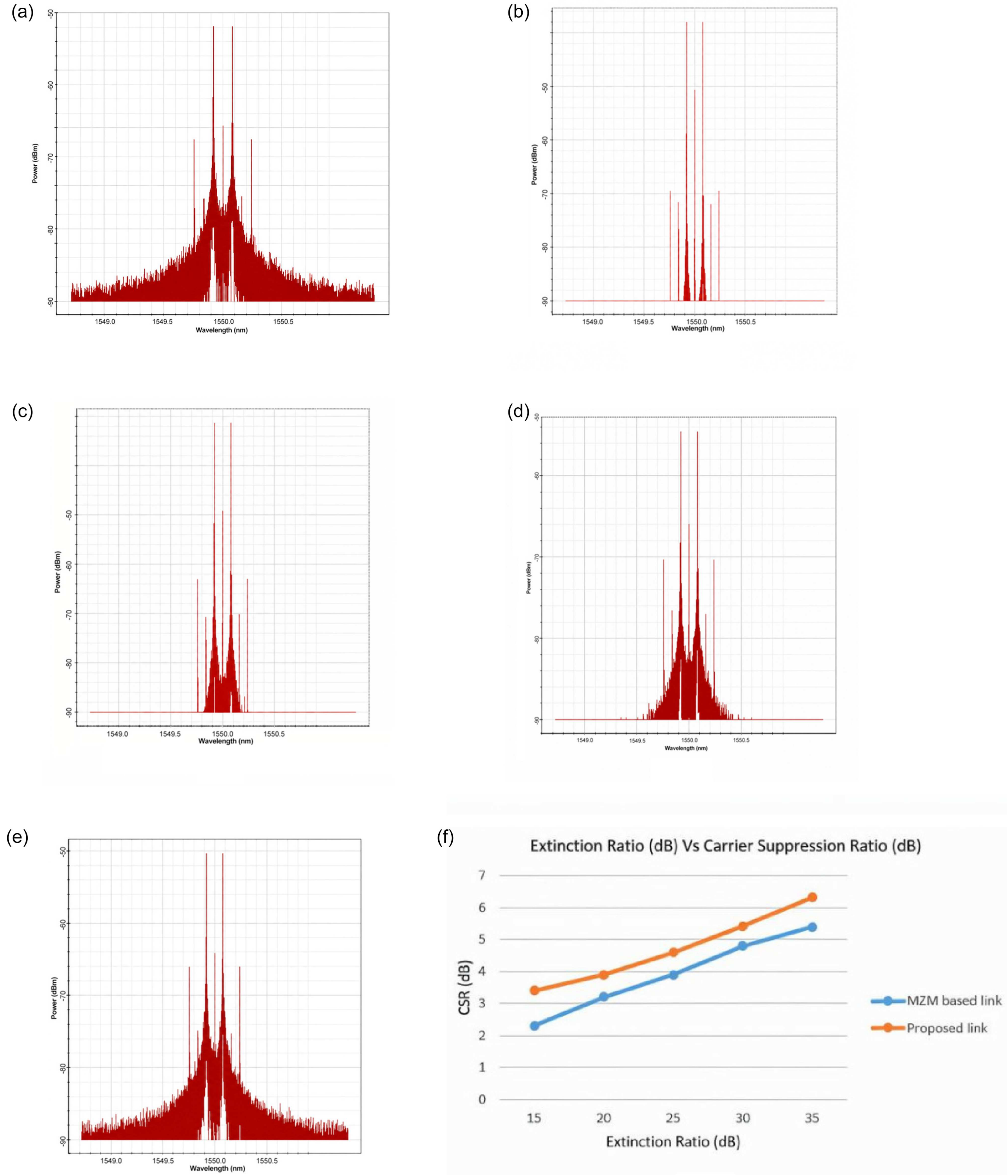

adjusting the polarization angle and aligning the polarizer, the carrier component is suppressed, and power fading is mitigated. The amplified optical signal is then passed through an EDFA operating in automatic power control mode, and the link is tested over a practical transmission distance of 50 km. The optical signal is finally converted to an electrical signal using a photodiode with a responsivity of 0.45 A/W.

Carrier suppression is verified through spectra obtained at the Sagnac loop output, as shown in Figure 2(a), where a suppression level of −49 dBm is observed. The modulator is biased to operate in an OCS regime, with a quadrature phase shift (90°) applied to enable single-sideband (SSB) modulation. This approach effectively reduces power fading, particularly at frequencies prone to destructive interference.

To assess frequency response, the RF input is swept from 2 GHz to 22 GHz. As illustrated in Figure 2(b), the conventional system shows significant power fading at 12 GHz and 18 GHz. In contrast, the proposed system maintains a nearly flat frequency response, indicating superior performance for broadband applications. The ER is further varied to examine its impact on OCSR. At 35 dB ER, the OCSR reaches 6.32 dB. A decrease in ER to 15 dB results in reduced OCSR (3.2 dB), demonstrating the sensitivity of carrier suppression to modulator biasing. Figure 3(a)–(e) show the modulated optical spectra for different ER values. The highest suppression is obtained at ER = 35 dB, consistent with the observed OCSR trend in Figure 3(f).

Figure 4(a) presents the electrical spectrum captured at the photodetector output, showing a maximum received power of −42 dBm at 10 GHz, validating effective RF transmission. Figure 4(b) depicts the optical spectrum at the EDFA output after 50 km transmission, confirming the system's viability for medium-range optical wireless links.

The system's linearity is benchmarked using SFDR, an essential performance metric in high-frequency RoF systems. Figure 5(a) shows SFDR values ranging from 100.23 to 98.34 dB.Hz$^{2/3}$ across 1–20 GHz, offering an enhancement of over 19 dB compared to conventional MZM-based links. This improvement is attributed to optimized carrier suppression and minimized intermodulation distortion (IMD3) in the proposed link.

EVM is measured for a 16-Quadrature Amplitude Modulation (QAM) signal modulated at 10 GHz. As RF input power increases from −20 dBm to 20 dBm, the EVM drops from 16.34%

Figure 4

Electrical spectra obtained at the output of the photodetector, showing the power level of the received signal. (b) Optical spectra obtained from the EDFA at a length of 50 km

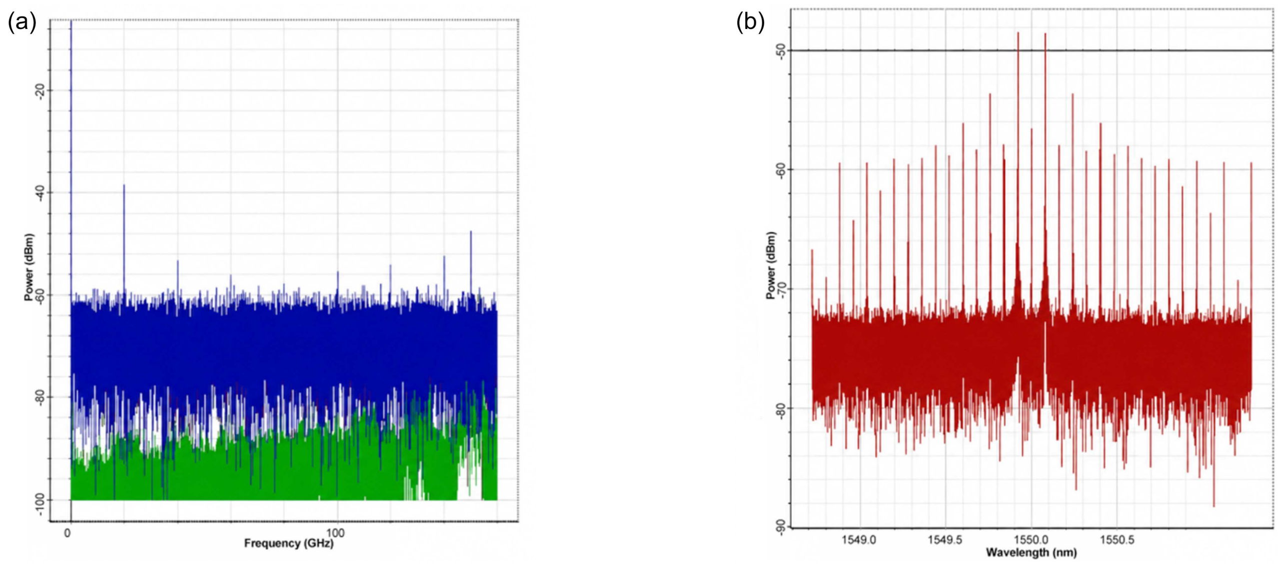

Figure 5

(a) Variation of SFDR with respect to frequency of the input signal (in GHz) and (b) variation of EVM (in %) with respect to power of the input signal (in dBm)

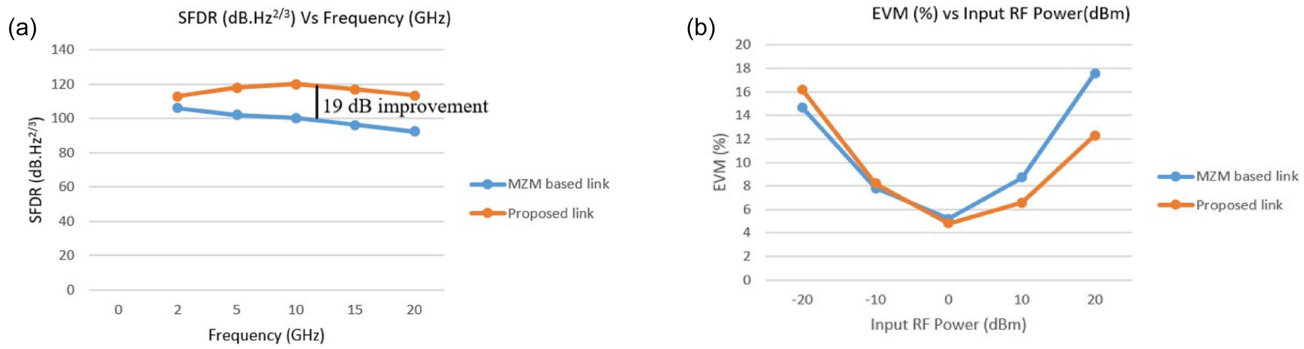

Figure 6
(a) Variation of BER with respect to power of the input signal (in dBm) and (b) variation of SNR (in dB) with respect to power of the input signal (in dBm)

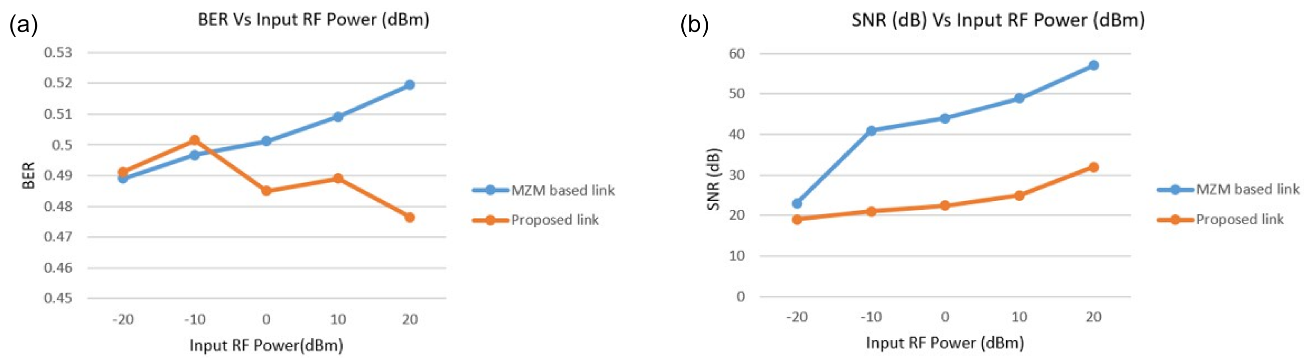

Table 1
Comparison of key parameters between the proposed system and traditional MZM-based systems

Parameter	Proposed system	Traditional MZM-based system
OCSR	6.32 dB at ER = 35 dB	3 dB (typical)
SFDR	98.34–100.23 dB.Hz$^{2/3}$	81–82 dB.Hz$^{2/3}$
EVM	12.56–16.34% (varies with power)	16.5% (typical)
BER	0.4734–0.4913	0.5 (typical)
Performance at high frequencies	Stable across frequencies (no fading)	Fading at 12 GHz, 18 GHz

to 12.56%, as shown in Figure 5(b), indicating improved signal fidelity under high power conditions.

BER and SNR are also evaluated as indicators of system reliability. Figure 6(a) shows a BER reduction from 0.4913 to 0.4734 as input power increases, while Figure 6(b) indicates that SNR varies from 16.45 dB to 12.45 dB over the same range [22]. Compared to traditional MZM-based links, the proposed architecture exhibits better BER stability due to effective nonlinear distortion mitigation through carrier suppression and polarization control [23].

The complete validation process involved testing the system under practical deployment conditions, including real optical components (laser, EDFA, photodiode) and varying modulation parameters [24, 25]. The proposed link maintained consistent performance across a 50 km transmission span, highlighting its potential for implementation in high-speed metropolitan or inter-building RoF networks. Table 1 shows the comparison of key parameters between the proposed system and traditional MZM-based systems.

4. Conclusion

In this paper, we proposed an optimized approach to improve the linear OCSR and compensate for power fading in a RoF link using a Sagnac loop configuration. The system's performance was evaluated using various metrics including ER, SFDR, BER, EVM, and SNR. The optical spectrum at the output of the Sagnac loop demonstrated effective carrier suppression, which improved consistently with increasing ER values—from 15 dB to 35 dB—resulting in a corresponding rise in CSR. The frequency response comparison highlighted superior performance of the proposed Sagnac loop system over the conventional MZM-based system. Electrical spectra from the photodetector output showed a strong received signal, and the optical spectra after 50 km fiber transmission confirmed stable signal integrity. The system exhibited an SFDR improvement of more than 19 dB, reaching a peak of 113.34 dB·Hz$^{2/3}$ at 20 GHz, as shown by the SFDR versus frequency analysis. Further, the system achieved a BER of 0.4765 and an SNR of 32 dB at higher RF input power levels. The EVM dropped to 12.31%, confirming effective power fading compensation. Plots of BER, EVM, and SNR versus input power support these observations. Overall, the proposed Sagnac loop-based RoF link demonstrates improved carrier suppression, dynamic range, and signal quality, outperforming conventional MZM-based systems and positioning itself as a strong candidate for high-performance RoF communication systems. Table 2 shows the comparison of the proposed RoF system with related works.

Table 2
Comparison of the proposed RoF system with related works

Reference	Technique used	Key performance metrics	Remarks
Zheng et al. [23]	Carrier Phase-Shift Pulse Width Modulation (PWM) in Permanent Magnet Synchronous Motor (PMSM) systems	Focus on harmonic suppression; limited to electrical domain	Not designed for optical carrier suppression or RoF applications
Chen et al. [19]	Standard MZM-based RoF link	OCSR 3 dB, SFDR 81–82 dB.Hz$^{2/3}$, BER 0.5, Power fading at 12/18 GHz	Performance degraded at higher RF frequencies due to two-sideband interference

(*Continued*)

Table 2
(*Continued*)

Reference	Technique used	Key performance metrics	Remarks
Zheng et al. [23]	Conventional RoF with no polarization control	EVM 16.5%, BER unstable, significant power-dependent distortion	Lacks robustness at high modulation indices and longer links
This work (proposed)	Optical Carrier Suppression + Polarization Control + SSB Modulation	OCSR = 6.32 dB, SFDR = 98.34–100.23 dB.Hz$^{2/3}$, BER = 0.4734, EVM = 12.56%, Stable from 2–22 GHz	Superior spectral efficiency, robust transmission over 50 km, ideal for high-speed RoF links

Ethical Statement

This study does not contain any studies with human or animal subjects performed by any of the authors.

Conflicts of Interest

The authors declare that they have no conflicts of interest to this work.

Data Availability Statement

Data sharing is not applicable to this article as no new data were created or analyzed in this study.

Author Contribution Statement

Archa Chandrasenan: Conceptualization, Methodology, Formal analysis, Resources, Data curation, Writing – original draft, Writing – review & editing, Visualization. **S. J. Anshula Vijayam:** Software, Supervision, Project administration. **Joseph Zacharias:** Validation, Investigation.

References

[1] Capmany, J., & Novak, D. (2007). Microwave photonics combines two worlds. *Nature Photonics*, *1*(6), 319–330. https://doi.org/10.1038/nphoton.2007.89

[2] Hua, Q., Zhang, Y., Wei, C., Ji, Z., Jiang, Y., Wang, Y., & Xu, D. (2023). A self-supervised method based on CV-MUNET++ for active jamming suppression in SAR images. *IEEE Transactions on Geoscience and Remote Sensing*, *61*, 5209516. https://doi.org/10.1109/TGRS.2023.3283135

[3] Yin, S., & Wang, X. (2023). A novel current harmonic suppression method for HSPMSG based on the hybrid rectifier. *IEEE Transactions on Transportation Electrification*, *9*(3), 4594–4604. https://doi.org/10.1109/TTE.2023.3243023

[4] He, J., Ye, Y., & Wang, X. (2023). ZVS and inrush charging current suppression design for switched-capacitor multilevel inverters. *IEEE Transactions on Power Electronics*, *38*(9), 10611–10616. https://doi.org/10.1109/TPEL.2023.3290570

[5] Qi, X., Liu, J., Zhang, X., & Xie, L. (2010). Fiber dispersion and nonlinearity influences on transmissions of AM and FM data modulation signals in radio-over-fiber system. *IEEE Journal of Quantum Electronics*, *46*(8), 1170–1177. https://doi.org/10.1109/JQE.2010.2044747

[6] Cui, Y., Dai, Y., Yin, F., Lv, Q., Li, J., Xu, K., & Lin, J. (2014). Enhanced spurious-free dynamic range in intensity-modulated analog photonic link using digital postprocessing. *IEEE Photonics Journal*, *6*(2), 7900608. https://doi.org/10.1109/JPHOT.2014.2308196

[7] Napoli, A., Mezghanni, M. M., Calabro, S., Palmer, R., Saathoff, G., & Spinnler, B. (2017). Digital predistortion techniques for finite extinction ratio IQ Mach–Zehnder modulators. *Journal of Lightwave Technology*, *35*(19), 4289–4296. https://doi.org/10.1109/JLT.2017.2729603

[8] Zhu, W., Gu, Y., Hu, J., Fan, F., Wu, Z., & Zhao, M. (2019). Dynamic range improvement of microwave photonic link based on destructive combination of nonlinear distortions. In *2019 International Topical Meeting on Microwave Photonics* (pp. 1–3). https://doi.org/10.1109/MWP.2019.8892019

[9] Wang, F., Shi, S., & Prather, D. W. (2019). Microwave photonic link with improved SFDR using two parallel MZMs and a polarization beam combiner. *Journal of Lightwave Technology*, *37*(24), 6156–6164. https://doi.org/10.1109/JLT.2019.2947230

[10] Gu, Y., & Yao, J. (2018). Microwave photonic link with improved dynamic range through π phase shift of the optical carrier band. *Journal of Lightwave Technology*, *37*(3), 964–970. https://doi.org/10.1109/jlt.2018.2884350

[11] Cui, Y., Dai, Y., Yin, F., Dai, J., Xu, K., Li, J., & Lin, J. (2013). Intermodulation distortion suppression for intensity-modulated analog fiber-optic link incorporating optical carrier band processing. *Optics Express*, *21*(20), 23433–23440. https://doi.org/10.1364/OE.21.023433

[12] Wu, R., Jiang, T., Yu, S., Shang, J., & Gu, W. (2019). Multi-order nonlinear distortions analysis and suppression in phase modulation microwave photonics link. *Journal of Lightwave Technology*, *37*(24), 5973–5981. https://doi.org/10.1109/JLT.2019.2943209

[13] Li, J., Zhang, Y.-C., Yu, S., Jiang, T., Xie, Q., & Gu, W. (2013). Third-order intermodulation distortion elimination of microwave photonics link based on integrated dual-drive dual-parallel Mach–Zehnder modulator. *Optics Letters*, *38*(21), 4285. https://doi.org/10.1364/OL.38.004285

[14] Lei, M., Zheng, Z., Qian, J., Xie, M., Bai, Y., Gao, X., & Huang, S. (2019). Broadband chromatic-dispersion-induced power-fading compensation for radio-over-fiber links based on Hilbert transform. *Optics Letters*, *44*(1), 155–158. https://doi.org/10.1364/OL.44.000155

[15] Tanaka, Y., Hara, K., Kanai, T., Kanazawa, S., Shindo, T., Nada, M., . . . , & Yoshida, T. (2024). Zero-dispersion wavelength estimation and optimization method for penalty-free and equalizer-free 53-Gbps/λ IM-DD transmission over 100 km. *Journal of Lightwave Technology*, *42*(6), 1844–1852. https://doi.org/10.1109/JLT.2023.3328588

[16] Wu, B., Wang, M., Tang, Y., Sun, J., Zhang, J., Yan, F., & Jian, S. (2017). Optical single sideband modulation with tunable optical carrier-to-sideband ratio using a modulator in a

Sagnac loop. *Optics & Laser Technology*, *91*, 98–102. https://doi.org/10.1016/j.optlastec.2016.12.006
[17] Zhao, H., & Zhang, Y. (2022). CWT-based method for extracting seismic velocity dispersion. *IEEE Geoscience and Remote Sensing Letters*, *19*, 7502205. https://doi.org/10.1109/LGRS.2021.3056610
[18] Yang, J., Wang, Y., Fang, Y., Geng, W., Zhao, W., Bao, C., . . . , & Yue, Y. (2022). 1. 3-octave coherent supercontinuum generation of OAM mode in ring-core fiber with all-normal dispersion. *IEEE Access*, *10*, 76990–76997. https://doi.org/10.1109/ACCESS.2022.3190631
[19] Chen, Z., Tu, X., Dai, M., Li, Q., & Fu, H. Y. (2022). Kerr frequency comb generation in microsphere resonators with normal dispersion. *Journal of Lightwave Technology*, *40*(4), 1092–1097. https://doi.org/10.1109/JLT.2021.3128996
[20] Chen, Y., Dai, H., Si, H., Wang, F., Wang, B., & Wang, L. (2022). Long-haul high precision frequency dissemination based on dispersion correction. *IEEE Transactions on Instrumentation and Measurement*, *71*, 5503207. https://doi.org/10.1109/TIM.2022.3214617
[21] Lou, S., Yang, Y., Liang, Y., & Wu, Y. (2022). Coordinated optimization of multi-energy generation systems considering the health damages of coal-fired pollutant dispersion. *CSEE Journal of Power and Energy Systems*, *8*(6), 1613–1622. https://doi.org/10.17775/CSEEJPES.2020.03770
[22] Xu, S., Yi, J., Hu, Y., Yang, H., Nong, J., & Wan, X. (2024). Experimental research on pseudo carrier-domain interference suppression of FM-based passive radar. In *2024 14th International Symposium on Antennas, Propagation and EM Theory* (pp. 1–4). https://doi.org/10.1109/ISAPE62431.2024.10841322
[23] Zheng, B., Zou, J., Xu, Y., Yu, G., Wang, L., & Zanchetta, P. (2024). High-frequency current harmonic analysis and suppression in dual three-phase PMSMs with advanced carrier phase-shift PWM. *IEEE Transactions on Power Electronics*, *39*(2), 2569–2581. https://doi.org/10.1109/TPEL.2023.3330934
[24] Pan, Q., Xu, H., Xu, H., & Quan, Y. (2024). A time-varying modulation interference suppression method based on mutual cancellation. In *2024 IEEE International Conference on Signal, Information and Data Processing*, 1–6. https://doi.org/10.1109/ICSIDP62679.2024.10868375
[25] Liu, J., Tang, Y., & Yu, J. (2024). BLDC sideband harmonic suppression based on carrier synchronization at commutation time. In *2024 IEEE 7th Student Conference on Electric Machines and Systems*, 1–6. https://doi.org/10.1109/SCEMS63294.2024.10756391

How to Cite: Chandrasenan, A., Vijayam, S. J. A., & Zacharias, J. (2026). Enhancing Carrier Suppression in Radio-over-Fiber Links Using Sagnac Loop Techniques. *Journal of Optics and Photonics Research.* https://doi.org/10.47852/bonviewJOPR62024617